IEEE Access
Multidisciplinary ⋮ Rapid Review ⋮ Open Access Journal

Received May 25, 2020, accepted June 11, 2020, date of publication June 17, 2020, date of current version June 29, 2020.

Digital Object Identifier 10.1109/ACCESS.2020.3003136

Coherent Plane-Wave Compounding Based on United Coherence Factor

CHEN YANG[1,2], JIE XU[2], YIWEN XU[3], YAOYAO CUI[2], (Member, IEEE), AND YANG JIAO[2]

[1]University of Science and Technology of China, Hefei 230052, China
[2]Suzhou Institute of Biomedical Engineering and Technology, Chines Academy of Sciences, Beijing 100864, China
[3]Suzhou Guoke Ultra Medical Technology Company, Ltd., Suzhou 215010, China

Corresponding author: Yang Jiao (jiaoy@sibet.ac.cn)

This work was supported in part by the Funds of Chinese Academy of Sciences under Grant YJKYYQ20180031, and in part by the foundation from Suzhou Institute of Biomedical Engineering and Technology, Chinese Academy of Sciences, under Grant Y85K021605.

ABSTRACT We present a united coherence factor beamformer for coherent plane-wave compounding (CPWC). CPWC is capable to reach an image quality comparable to the conventional B-mode imaging with a much higher frame rate and could be further applied to Doppler imaging. Conventional coherence factor (CF) based beamformers for CPWC use only either the spatial coherence or angular coherence information, which limits the image quality. To take full advantage of the radio frequency (RF) data for better image quality, this paper proposes a united coherence factor (uCF) using both spatial and angular information for CPWC. The proposed uCF is applied to simulated, phantom and *in vivo* imaging data. We evaluate the performance of the proposed method by lateral resolution and contrast. For simulated images, the contrast ratio (CR) improvements are over 80%. In the phantom images, the maximum improvements of the lateral full width at half maximum (FWHM) and CR are 10% and 105%, respectively. To compare the most core differences, the spatial and angular methods are also presented in this paper. uCF is superior in lateral resolution improvement and contrast among the beamformers. In addition, the proposed uCF performance also shows good performance in the power Doppler experiment with improved image quality, which is further verified by the spatial similarity matrix of the Doppler image. Thus, the proposed method (uCF) has a great potential to be applied in CPWC for image quality improvement.

INDEX TERMS Coherent plane-wave compounding (CPWC), spatial and angular coherence, united coherence factor.

I. INTRODUCTION

Medical ultrasound is a major imaging modality with the low cost, safety and real-time features. It has been widely used in clinical diagnose and treatments. Generally, the frame rate of a clinical ultrasound machine is limited to around 30 frames per second (fps) due to the line-per-line acquisition of the transmitted ultrasound signals. Increasing the frame rate will pave the way to superior applications which needs to record transient events, such as the motion and transient elastography [1], [2]. Many groups conducted related research to reach high frame rate. Lu and Greenleaf [3] proposed the application of nondiffracting beams in 1990s, and Fink [4] proposed the concept of ultrafast ultrasound imaging with plane wave. Among these methods, the plane-wave imaging (PWI) proposed by Fink received extensive attention and further investigations have been made to increase the frame rate [1].

PWI scans the whole region of interest by transmitting plane (or unfocused) waves, instead of the focused beam using the line-per-line acquisition. The frame rate of PWI could exceed 1000 fps, however, at the expense of the degradation of image quality [5]. To balance the frame rate and image quality, a coherent compounding method with several steering-plane-wave transmissions is proposed by Montaldo *et al*. [1]. The coherent plane-wave compounding (CPWC) makes a good compromise between imaging quality and frame rate and has made great contributions to the development of the advanced medical ultrasound [2], [5], [6]. Without compromising image quality comparing with conventional focused mode ultrasound, the frame rate can be increased by 5-10 times using CPWC. In addition to its use in tissue imaging, CPWC also leads to large progress in Doppler-based flow analysis methods, which also require

The associate editor coordinating the review of this manuscript and approving it for publication was Hasan S. Mir.

This work is licensed under a Creative Commons Attribution 4.0 License. For more information, see https://creativecommons.org/licenses/by/4.0/

high frame rates [2], [6], [7]. By replacing the line-per-line method to CPWC, the Doppler-based techniques could get all the information of the imaging region in a short time which make the high-precision characterization of complex vascular and blood flow possible.

By the coherent compounding method, the image quality is improved and is negatively correlated with the frame rate: the higher the number of imaging angles, the better the image quality; but at the same time, the frame rates will be lower [5]. Theoretically, the frame rate of CPWC with single angle transmission, which is the same as PWI would drop down by N times where N is the total number of the steering-plane-wave transmissions in CPWC.

In addition to the coherent compounding, Montaldo *et al.* also applied the delay-and-sum (DAS) to CPWC. The framework incorporating both DAS and multi -angle-coherent-compounding was then accepted as a standard method [8]. Due to the compromise between imaging quality and frame rate, the image quality couldn't be enhanced by increasing the number of angles unlimitedly. Meanwhile, the DAS algorithm in CPWC only uses the simple addition of data in the delay line. To improve the spatial and contrast resolution without decreasing frame rate (increasing angle number), many beamformers were introduced to DAS.

Among the beamformers, the minimum variance beamforming and coherence-based beamforming are two of the most representative methods [9]. The minimum variance (MV) beamformer was first proposed in the1960s [10] and Synnevag *et al.* applied the method to the field of ultrasonic imaging [11]. Since then, MV has been comprehensively investigated in ultrasound imaging [11]–[13]. MV could increase the lateral resolution and contrast. However, it also requires a large number of computing resources [11]. Meanwhile, because of the better image quality and lower computational load, the coherence based beamforming was also widely researched and applied in ultrasound [14], [15].

Previous coherence based beamforming was adapted from the van Cittert Zernike (VCZ) theorem, which describes the spatial coherence of backscattered waves in ultrasound imaging [16]. It is computed as a ratio of coherent across the channel signals (like a spatial filter) which differs in space and has been widely applied in B-mode, CPWC and photoacoustic imaging [17]–[19]. The spatial coherence has also been applied to blood flow detection, which could increase the contrast between blood flow and tissues [20].

Besides the spatial coherence, the angular coherence beamformer has also been studied. The angular coherence theory could be seen as a supplementary form of the spatial coherence theory [21]. Due to the characteristics of multi-angle transmission in CPWC, angular coherence have also been applied to CPWC in recent years [21], [22]. The angular method improves image quality and greatly reduces the amount of calculation compared to the spatial coherence method. Both the spatial and angular methods could improve image quality in CPWC. Meanwhile, the spatial method pays more attention to the correlation of different element signal, and the angular focuses more on the correlation of different steering plane-waves.

The spatial and angular methods have been the mainstream of the coherence methods. However, neither of them takes advantage of the other's correlation, which limits their further improvement in imaging quality. In this work, we present a coherence factor which unites the spatial correlation and angular correlation. To highlight the differences from the spatial and angular coherence factor, we name the new method united coherence factor (uCF). In the proposed approach, the correlation of a point in CPWC image will be obtained uniformly using all the signals in the CPWC to calculate the point, instead of calculating separately by space or angle.

We use CPWC, spatial coherence factor (sCF) and angular coherence factor (aCF) as comparison methods for the proposed uCF method and apply on simulated, phantom, and *in vivo* data sets to show all the beamforming's effect in grayscale imaging. To show the noise suppression capability of the uCF intuitively, we also applied it to the power Doppler imaging and performed singular value decomposition (SVD) analysis on the results.

In the following section, we first introduced the comparisons between the united coherence factor beamformer and other conventional methods, especially the spatial and angular methods. To show the differences in the imaging quality of these methods, we applied the beamformers to the data acquired from the simulation, phantom, *in vivo* and Doppler study. The acquisition parameters for these studies and the imaging results are shown in Section V and Section IV, respectively. The imaging results are explained and analyzed in Section V. Finally, conclusions are given in Section VI.

II. METHODS

A. PROPOSED COHERENT PLANE-WAVE COMPOUNDING

CPWC was proposed to improve the image quality by coherent synthetic summation of ultrasonic images acquired with plane waves at different steering angles [1]. Each point *(x,z)* of a steering angle (α_i) in the image region could be expressed as:

$$X_c^i(x, z) = \frac{1}{M} \int_{j=1}^{j=M} RF(x_j, \tau(x, z, x_j)) \tag{1}$$

where M is the element number of the aperture which depends on the F-number and j stands for the index of the channels in the aperture of transducer. The delay τ changes with different angles α_i, $i = 1, 2 \ldots N$, where i is the angle index and N is the total number of the steering angles.

Let X_c be the compound data of the point *(x,z)*. It could be given as [1]:

$$\begin{aligned} X_c(x, z) &= \frac{1}{N} \sum_{\mathrm{i}=1}^{N} X_c^i(x, z) \\ &= \frac{1}{MN} \sum_{\mathrm{i}=1}^{N} \sum_{\mathrm{j}=1}^{M} RF(x_j, \tau(x, z, x_j)) \end{aligned} \tag{2}$$

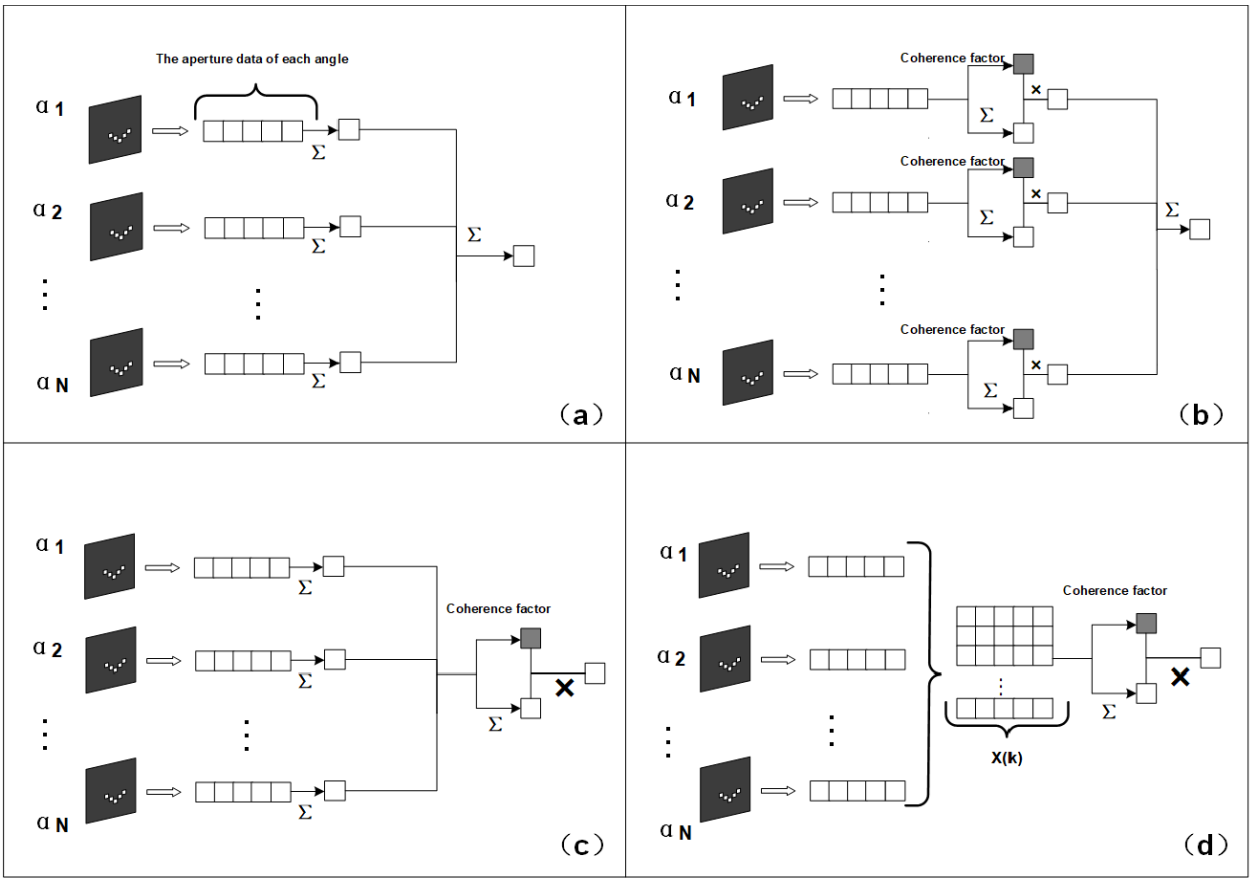

FIGURE 1. Diagrams of the beamformer frameworks. (a) CPWC, (b) the sCF method, (c) the aCF method, (d) the uCF method. The symbol $\sum$ represents the process of averaging data. The symbol X represents the process of multiplication.

The position index (x, z) is a two-dimensional index that changes with lateral and longitudinal position. For convenience, we can replace it with the discrete 1D index k. The signals for the specific point with the index k, after appropriate phase rotation, could be arranged in the form of a matrix of $N \times M$ [1],

$$X(\mathrm{k}) = \begin{pmatrix} x_{1,1}(\mathrm{k}) & \cdots & x_{1,M}(\mathrm{k}) \\ \vdots & \ddots & \vdots \\ x_{N,1}(\mathrm{k}) & \cdots & x_{N,M}(\mathrm{k}) \end{pmatrix} \tag{3}$$

where $x_{i,j}(k)$ is the RF signal received by the channel j at steering angle i. In the DAS method, we could obtain the X_c (2) in the discrete form:

$$X_c(\mathrm{k}) = \frac{1}{MN} \sum_{i=1}^{N} \sum_{\mathrm{j}=1}^{M} x_{i,j}(\mathrm{k}) \tag{4}$$

More details about CPWC could be found in [1] and Fig. 1(a) shows its diagram.

B. PROPOSED SPATIAL AND ANGULAR COHERENCE FACTOR BEAMFORMERS

Coherence Factor (CF) beamformer was first used in conventional focused ultrasound [17], and it calculates the correlation between the magnitude of the channels across the aperture [23]. The coherence factor in the focused ultrasound could be calculated as:

$$CF\,(k) = \frac{\left| \sum_{j=1}^{M} x_j(k) \right|^2}{M \sum_{j=1}^{M} \left| x_j(k) \right|^2} \tag{5}$$

With the development of the ultrafast ultrasound, CF was quickly applied to CPWC. As CF is computed as a ratio of coherent to the average result of DAS across the channel signals which differs in space, CF used in CPWC also works as a spatial filter. To underline its resemblance with the 'spatial' filter, we name it the spatial coherence factor (sCF) as mentioned before, and the sCF calculation could be shown as:

$$sCF_i\,(k) = \frac{\left| \sum_{j=1}^{M} x_{i,j}(k) \right|^2}{M \sum_{j=1}^{M} \left| x_{i,j}(k) \right|^2} \tag{6}$$

where the subscript i of $sCF_i(k)$ implies that the sCF is different within every steering angle. A low factor value indicates low directionality or a low-quality image. And the sCF beamformer output is:

$$Y_s(\mathrm{k}) = \frac{1}{N}\sum_{i=1}^{N} sCF_i(k)\, X_c^i(\mathrm{k}) \tag{7}$$

Besides the spatial coherence, Li [21] also introduced the efficiency of the angular coherence for CPWC in recent years. Based on the angular coherence theory [21], the angular coherence factor beamformer (aCF) focuses more on the similarity among the images with different steering angle. Its calculation and output could be described as:

$$aCF(k) = \frac{\left|\sum_{i=1}^{N}\frac{1}{M}\sum_{j=1}^{M} x_{i,j}(k)\right|^2}{N\sum_{i=1}^{N}\left|\frac{1}{M}\sum_{j=1}^{M} x_{i,j}(k)\right|^2} \tag{8}$$

$$Y_a(\mathrm{k}) = \frac{1}{N} aCF(\mathrm{k})\sum_{i=1}^{N} X_c^i(\mathrm{k}) \tag{9}$$

Corresponding to $Y_s(\mathrm{k})$, the subscript a of $Y_a(\mathrm{k})$ means 'angular'. The diagrams of sCF and aCF beamformer are shown in the Fig.1 (b) and (c), respectively.

C. THE UNITED CF FOR CPWC

The sCF and aCF methods both use the amplitude correlation of the RF data to multiply the DAS result as a scaling factor. Omitting the same 'coherence factor', their differences for CPWC are mainly reflected in the 'spatial' correlation between the channels of the aperture or the 'angular' correlation between the angles. Although the angular coherence reduced computational complexity, it is also limited by the angle number and frame rate. Thus, the spatial coherence is still necessary to increase image quality [24].

Discrete signals X(k) from different channels and angles representing point (x,z), which contains all informaiton of the corresponding point, and all the elements of X(k) are equally weighted in the DAS method. However, as shown in Fig1. (b) and (c), sCF calculates the scaling factor within each row of X(k), and aCF calculates the factor from the sums of each row along the remaining columns. The coherence of the two methods (sCF and aCF) don't set the weights of all the elements of X(k) equal and the two methods ignore the coherence from the other.

Thus, we propose a beamformer combining both the spatial coherence and angular information. We would show that the new method has better image quality compared to the spatial and angular methods in the following sections. The analysis of the performance would also be discussed in Section V.

In the new beamformer, the beamforming coherence factor could be calculated by all the elements of X(k) and applied to the average result of CPWC. It acts like a united filter containing both the spatial and angular coherence. The united coherence factor (uCF) could be calculated as:

$$uCF(k) = \frac{\left|\sum_{i=1}^{N}\sum_{j=1}^{M} x_{i,j}(k)\right|^2}{NM\sum_{i=1}^{N}\sum_{j=1}^{M}\left|x_{i,j}(k)\right|^2} \tag{10}$$

As mentioned before, all elements in the matrix X(k) are weighted equally in the calculation of the united coherence factor. In the calculation process, uCF calculates the coherence of all the elements other than the coherence in every fractional row (sCF) or the coherence among the sum of every row (aCF). This is also the core difference between it and the other two methods.

The united coherence factor also has a value between 0 and 1. A high uCF value indicates that the ultrasonic field is highly directional, i.e., highly likely to be a scatterer. A low value indicates low directionality or highly likely to be noise. This yields the uCF output:

$$Y_u(\mathrm{k}) = \frac{1}{N} uCF(\mathrm{k})\sum_{i=1}^{N} X_c^i(\mathrm{k}) \tag{11}$$

By enhancing the signal of high-quality echo points while weakening the signal of low-quality echo points (with noise), the uCF could improve the image quality and Fig. 1(d). shows the diagram of the proposed method.

TABLE 1. Imaging parameters.

Parameter	Value
Pitch	0.3mm
Element width	0.27mm
Number of elements	128
Transmit frequency	7.8M[Hz]
Sampling frequency	30M[Hz]
F-number	1.75

III. SIMULATION AND EXPERIMENT

A. ACQUISITION PARAMETERS

To verify the performance of the proposed method, we used data from the simulation, phantom, *in vivo* and Doppler experiment. The simulated data were acquired with the ultrasound simulation program Field II [25], [26]. The mimicking phantom, in *vivo* and Doppler datasets were recorded using a Verasonics Vantage 64LE research scanner and L11 probe (Verasonics Inc., Redmond, WA, USA). To make the parameters consistent, we also used the same settings in the simulation as in the experiment. The imaging parameters are shown in TABLE 1, and each image acquisition (both simulated and experimental) includes the transmission of 11 plane waves with steering angles spaced uniformly between $-18°$ and $18°$, which is also the recommended parameters of Vantage.

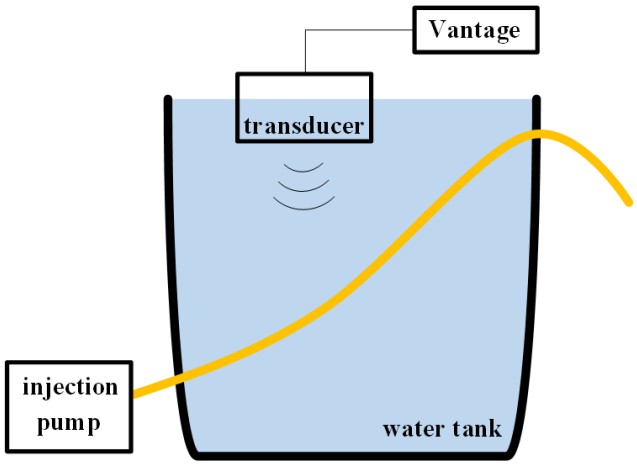

FIGURE 2. Doppler experimental setup.

The simulation includes the point-target and anechoic-cysts datasets, which could be shown in Fig. 3 and 5, respectively. The mimicking phantom has isolated nylon scatters and two anechoic cysts, whose distribution is shown in the Fig. 6. The speed of sound in the mimicking phantom is 1540 ± 10 m/s with a background attenuation of 0.70 ± 0.05 dB/cm/MHz, and the *in-vivo* data we used is from a carotid artery.

Ultrafast Doppler imaging based on plane-wave imaging is greatly affected by the beamforming result. We also designed a power Doppler experiment for analysis to further illustrate the effect of uCF. We used a 5mm inner diameter tube filled with blood-mimicking fluid. The fluid circulation was insured by a homemade variable-speed tubing pump and the experiment designed is shown in the Fig.2.

B. EVALUATION METRICS

We compare the proposed method in terms of spatial resolution and contrast resolution. For spatial resolution, we use the criteria full width at half maximum (FWHM, -6 dB beam width) [27] and for contrast resolution, the contrast ratio (CR) [27] and generalized contrast-to-noise ratio (gCNR) were measured.

Both the axial and lateral resolution could be measured to evaluate the performance of each beamformer. Because the CF-based beamformers are developed based on an assumption of narrow-band signals that ignores temporal correlation, the improvement in spatial resolution is mainly reflected in the lateral direction. Thus, we are interested in FWHM of the response in the lateral direction only.

The contrast resolution is often measured using the criteria CR and contrast-to-noise ratio (CNR), which is given by [27]:

$$CR = 20\ \log_{10}(\frac{\mu_{ROI}}{\mu_B}) \tag{12}$$

$$CNR = 20\log_{10}(\frac{\mu_{ROI} - \mu_B}{\sqrt{\sigma_{ROI}^2 + \sigma_B^2}}) \tag{13}$$

where μ_{ROI} and μ_B stand for the a value of the beamformed envelope signal over the region of interest and background, respectively. σ stands for the standard deviation of the signal of the area marked by subscript. CNR has been widely used in recent years. However, Rodriguez-Molares [28] proved that the CNR couldn't be used with modern beamformers, as dynamic range alterations can produce arbitrarily high CNR values with no real effect on the probability of lesion detection. Thus, we use gCNR [28] as a replacement for CNR. gCNR is robust against dynamic range and provides a quantitative measure for contrast. It is given by the equation:

$$\mathrm{g}CNR = 1 - \int min(p_B(x), p_{ROI}(x))dx \tag{14}$$

where x is the pixel intensity, p_B and p_{ROI}, are the probability distribution of the background and the region of interest (ROI). The overlap area of p_B and p_{ROI} represents their classification difficulty of their corresponding areas. If both p_B and p_{ROI} overlap completely, gCNR would equal to zero and this corresponds to the worst possible classification [28].

C. SIGNAL AND IMAGE PROCESSING

All the beamformers for tissue imaging and Doppler imaging are performed on RF data to generate envelopes with 5th order Butterworth filter.

Power Doppler image was obtained after IQ demodulation and clutter filtering. In many clutter filtering techniques, we chose SVD filter for its better performance in suppressing clutter signals, because SVD filtering is very robust compared to classical Fourier based clutter filters, such as finite impulse response (FIR) or infinite impulse response (IIR) filters which fail to discriminate flow and tissue when they have comparable speed and share overlapped spectrum [7]. The thresholds for singular values were chosen to provide the best image quality for all the methods, respectively. SVD can also provide analysis about the correlation of spatial singular vectors which reflect the quality of B-mode, which we would discuss in Section V. More about the SVD filter is beyond the scope of this article, and they could be found in [7].

IV. IMAGING DATA AND RESULTS

A. SIMULATION: POINT TARGETS

We start with an image of a point-reflector phantom obtained by the simulation. Fig. 3(a)-(d) shows the simulated point target images created by different methods with a dynamic range of 70 dB. 24 points are regularly distributed in the range of 25mm in width and 30mm in depth. Although the noise could be suppressed by CPWC, there still exists evident grating lobe artifacts and noises in Fig. 3(a). Compared with CPWC, all the CF-based beamformers show their ability to reduce the artifacts in Fig.3 (b)-(d), and the proposed uCF beamformer outperforms other methods with the visually cleaner background.

To show the performance of the beamformers in details, the lateral cross section of two middle points located at a depth of 10 mm and 20mm are shown in Fig. 4, respectively.

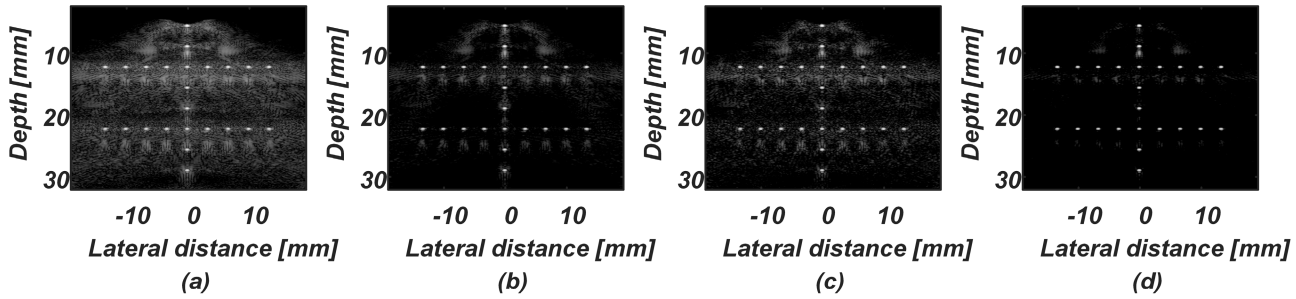

FIGURE 3. Simulated point images of different methods. (a) CPWC, (b) sCF, (c) aCF, (d) uCF. All images are shown in a 70 dB dynamic range.

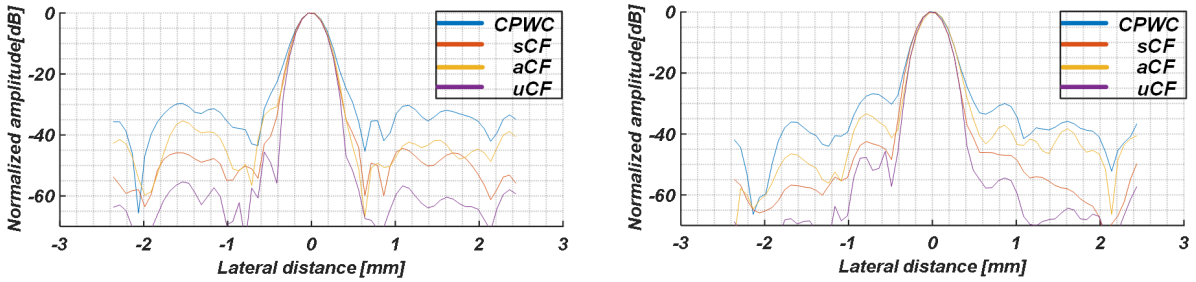

FIGURE 4. The lateral variations of the selected points in the simulated images at various depth,the left one (10mm),the right one (20 mm).

TABLE 2. Contrast performance from simulation.

beamformer	FWHM (mm) (simulation)	CR (dB) (simulation)			gCNR (simulation)		
		15mm depth	25mm depth	35mm depth	15mm depth	25mm depth	35mm depth
CPWC	0.39	7.60	11.64	13.35	0.70	0.75	0.80
sCF	0.36	7.77	14.59	17.29	0.64	0.87	0.86
aCF	0.36	13.72	16.12	19.86	0.80	0.81	0.84
uCF	0.34	16.87	21.59	26.27	0.85	0.89	0.90

As seen from Fig 4, uCF has the narrowest signal width and lowest noise level, which means better lateral resolution and better side lobe level. Except for the two selected points, we also measured the lateral FWHMs of all points and the average results are shown in Table 2. Consistent with the results of Fig. 3 and 4, the *uCF* method has the lowest FWHM which means the best lateral resolution. It improves lateral resolution (12%) over the CPWC result.

B. SIMULATION: CYST

Fig. 5 shows the three-simulated-cysts images with different beamformers. The dynamic range is also 70 dB. As shown in Fig. 5(a), there are some artifacts in the cyst region where signals should not appear. The ability to suppress artifacts in the cyst represents the contrast resolution of the corresponding method image. The cysts in Fig. 5(b)-(d) are more visible with noise suppression level inside, compared with that in Fig. 5(a).

To quantitatively measure the contrast resolution, we choose the metrics CR and gCNR as mentioned before. We utilized the data in the cyst, and the background of the same size area to compare the contrast resolution of the beamformers. The results for three different depth cysts are also listed in Table 2. The new method uCF also performs best among all the beamformers, it can offer CR improvements by 121% (15-mm-depth), 85% (25-mm-depth), 96%(35-mm-depth) over CPWC. The improvement of uCF on gCNR also exceeds 10% over CPWC.

C. PHANTOM STUDY

The images generated on the phantom data with different beamformers are shown in Fig. 6. The nylon targets and

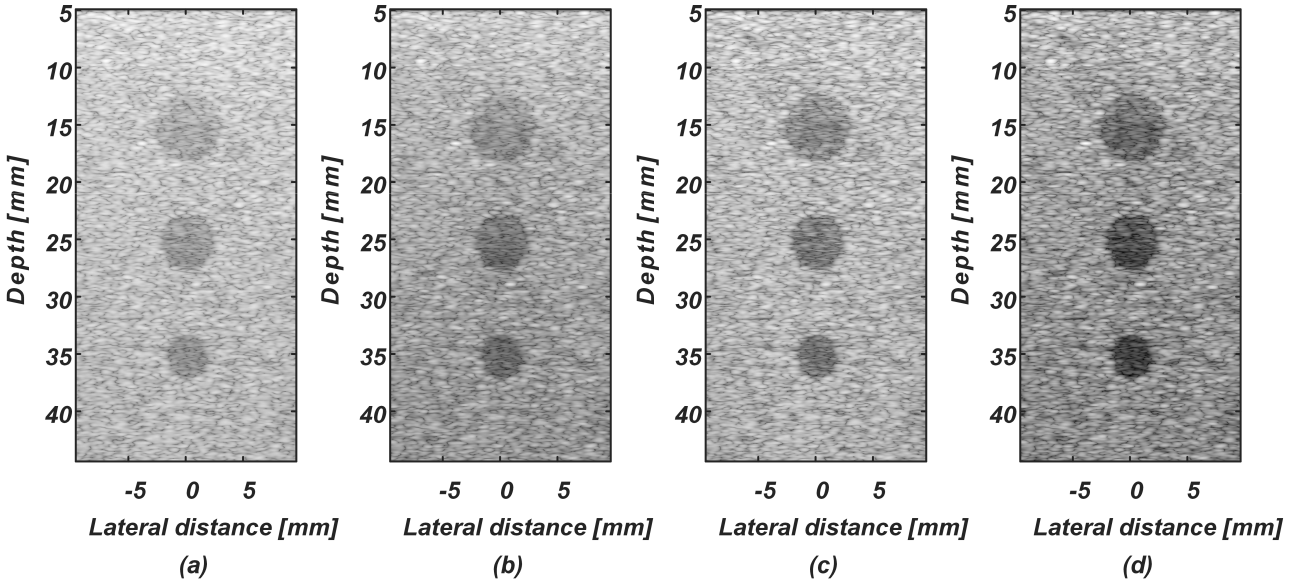

FIGURE 5. Simulated cyst images of different methods. (a) CPWC, (b) sCF, (c) aCF, (d) uCF. All images are shown in a 70 dB dynamic range.

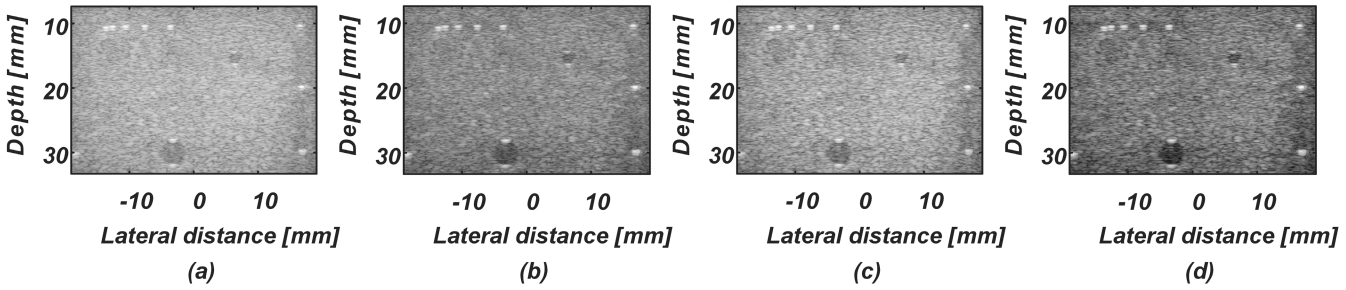

FIGURE 6. Phantom images of different methods. (a) CPWC, (b) sCF, (c) aCF, (d) uCF. All images are shown in a 70 dB dynamic range.

TABLE 3. Contrast performance from phantom, and *in vivo*.

beamformer	FWHM (mm) (phantom)	CR (dB) (phantom)		gCNR (phantom)		CR (dB) (*in vivo*)	gCNR (*in vivo*)
		15mm depth	30mm depth	15mm depth	30mm depth		
CPWC	0.69	6.57	7.10	0.54	0.47	6.52	0.59
sCF	0.63	8.26	10.36	0.58	0.59	11.42	0.78
aCF	0.64	9.39	10.20	0.56	0.52	10.74	0.74
uCF	0.62	11.18	14.56	0.59	0.65	15.25	0.80

two anechoic cysts (15-mm-depth and 30-mm-depth, respectively) are designed to enable the assessment of the lateral and contrast resolution, respectively.

Compared with the CPWC result, images generated by the CF-based beamformers also show better image quality and uCF still performs best as the point targets and cysts are easier to distinguish in the background. For each beamformer, we also measured the average FWHM, CR and gCNR which is shown in Table 3.

As for the contrast resolution, uCF could offer CR improvements by 4.61dB (70%) and 7.10 dB (105%) over CPWC. The gCNRs of two cysts also have been improved (over 9%), which means a greater ability to distinguish cysts from the background.

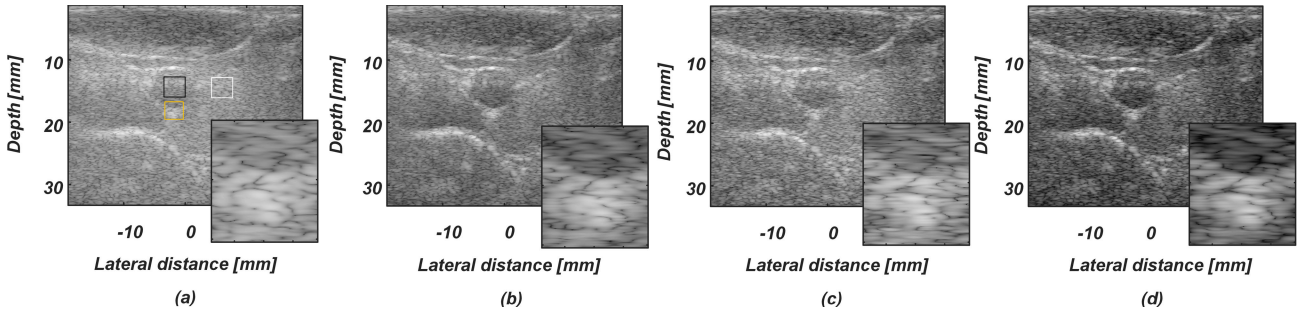

FIGURE 7. *In vivo* images of different methods. (a) CPWC, (b) sCF, (c) aCF, (d) uCF. All images are shown in a 70 dB dynamic range.

Similar to the contrast resolution, the FWHM of uCF is also slightly lower than that generated with other beamformers, which means a better lateral resolution. Thus, the new method uCF performs best in all the metrics.

D. IN VIVO STUDY

Due to the complex structure of biological tissue, the ultrasound signal would be more complicated compared with the simulation and phantom. Thus, we also applied the proposed beamformers to *in vivo* datasets of a carotid artery and Fig. 7 shows the ultrasound image results with a dynamic range of 70 dB.

The image quality of carotid arteries is generally measured by the contrast of the carotid arteries and the clarity of the boundaries. We evaluated the contrast of the beamformers by the quantitative metrics CR and gCNR. The results are also shown in Table 3. We take the artery as ROI (black box) and surrounding tissues as background (white box). uCF can offer CR improvements by 8.73 dB (133%) and gCNR improvements by 35% over CPWC. It could also increase CR by 33% compared with the best method of traditional methods (sCF).

The boundary clarity of the artery region and background could also reflect the effect of beamformers. Each boundary image is displayed in an enlarged view of the area surrounded by the yellow square. Among the results, all the boundaries of the CF-based beamformers are clearer than CPWC and the *uCF* beamformer has the clearest boundary. However, the CF-based beamformers also weaken the overall brightness of images. To show whether the method could remain the signal information, especially the arterial blood flow information while weakening the noise, we designed the power Doppler experiment in next subsection E.

E. DOPPLER

The performance of beamforming will greatly affect the results of power Doppler imaging and we could also judge the beamforming quality by the power Doppler Imaging performance analysis.

In order to further analyze the beamforming through power Doppler results, we designed the fluid experiment shown in the Fig.2. We used 135 frames of beamformed signals to get the power Doppler image.

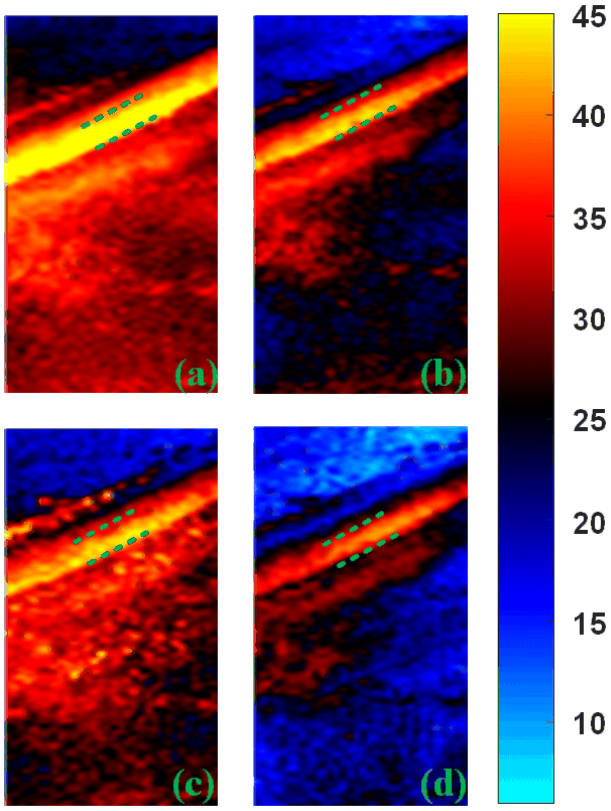

FIGURE 8. Power Doppler images of different methods. (a) CPWC, (b) sCF, (c) aCF, (d) uCF.

After SVD filtering, we could compare the beamformers' performance based on the power Doppler results. The inner wall of the tube is marked by the green line. Compared with the grayscale image, it can distinguish noise and signal more intuitively by color. The power Doppler results of different beamformers are shown in Fig. 8. After the SVD filtering, there should be only flow signal in the image without canal wall signal and noise. It should be highly noticed that the power Doppler image of CPWC still has many artifacts around the tube, which could be caused by the tube motion.

With CF-based beamformers, the flow component of the image would be clearer with less noise and uCF gets the

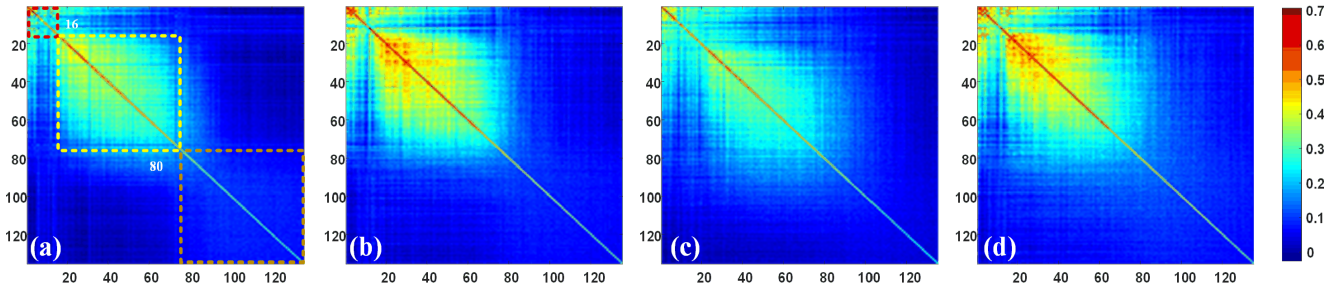

FIGURE 9. Spatial similarity matrices of different methods. (a)CPWC, (b) sCF, (c) aCF, (d) uCF.

best image quality. The uCF beamformer retained the flow signal while removing most of the noise, which means better discrimination of flow compared to other beamformers. Compared with the results in the *in vivo* study, the results of uCF could be considered that although the overall brightness has decreased, the most important blood flow information is still retained and more obvious with the united method (uCF).

V. DISCUSSION

A. THE COMPARISON OF DIFFERENT BEAMFORMERS

As shown in the simulation and experimental results, the uCF performs best in suppressing sidelobes and noise levels. The result could be explained by the different methods to calculate the coherence factor. Every point in the CPWC image can be considered as obtained by matrix X(k) (3). As shown in Fig.1(a), DAS singularly calculated the average of the matrix which makes it susceptible to noise interference. sCF calculates the coherence factor within every row of X(k) and aCF obtains the factor after adding the entries in each row along the remaining column. They both improve the imaging quality to some extent, but the calculation of coherence factors is equivalent to weight all elements of X(k) unequally. To make full use of X(k), the weight values of all elements in the matrix should also be the same in the calculation, which could also be considered as the combination of spatial coherence and angular coherence. Thus, uCF performs best among the beamformers.

The performance instability of aCF is also worth noting. Although the aCF could significantly reduce the amount of calculation, its performance declined in the Doppler experiment. This is mainly related to the correlation between frames which is reduced in the moving objects [29]. Although the time between frames in CPWC is short, the acquisition time of the first and last frames of each image is greatly increased compared with the acquisition time of one frame and it is positively linear correlated with the number of steering angles. For moving objects such as fluids, the correlation in the time dimension is significantly reduced compared to stationary objects, which causes a decline in aCF performance. Meanwhile, because of the use of spatial coherence, sCF and uCF performs well in the Doppler experiment.

TABLE 4. Computational complexity for one sample.

Beamformer	Addition Floating-point Operations	Multiplication Floating-point Operations
CPWC	MN	0
sCF	$2MN$	N
aCF	$MN+N$	1
uCF	$2MN$	1

B. THE ANALYSIS OF DOPPLER EXPERIMENT

We have used power Doppler experiments to further verify the effectiveness of the new method uCF. The source of CF-based performance improvement in Doppler is the suppression of thermal noise (i.e., electronic noise), which is spatially and temporally incoherent. It also appears as a white noise process. Li [20] also guessed that the stationary clutter also has lower coherence than the flow signal. Thus, the CF-based methods could improve the power Doppler imaging quality by suppressing the low-coherence signal. As mentioned before, the decline in *aCF* performance compared to *sCF* also reflects in the Doppler image. Larger time interval weakens the discrete flow signal coherence to the noise level, which decrease the image quality.

We used spatial similarity matrices of the Doppler experiment to further illustrate the Doppler performance of the four beamformers. The number of rows of the spatial similarity matrix is equal to the number of frames used for Doppler calculation (In this paper, it's 135). For ultrafast Doppler acquisition on a flux phantom after SVD decomposition, there would be three highly correlated areas in the matrix of spatial singular vectors. In Fig. 9(a), from 1 to 18 (red dotted squares), vectors describe the tissue and the canal walls. From 18 to 80 (yellow dotted squares), spatial vectors represent the blood flow signal. From 80 to 135, spatial vectors describe mostly noise. The three highly correlated areas represent information of tissue, flow and mostly noise. The magnitude of each area in this matrix represents how much the corresponding component is.

Fig. 9 shows the spatial similarity matrix of every beamformer and we could easily distinguish the three areas

in Fig. 9. The noise area in matrices of sCF and uCF is reduced while the flow area is more enhanced which means they show better effect in terms of noise reduction. However, the flow area in *aCF* matrix is also weakened because of the larger time interval, which could also match the result of Fig. 9.

C. THE COMPUTATIONAL COMPLEXITY OF THE BEAMFORMERS

As mentioned in Section II, the parameter M and N stands for the number of channels and the number of steering angles, respectively. The computational complexity of the image region is proportional to the number of samples of the region and we use the floating-point operations of every sample to evaluate the computational load.

The addition and multiplication floating-point operations of the beamformers are shown in Table 4. The number of floating operations in uCF is between sCF and aCF. However, because of the computational parallelism between the coherence factor and DAS result, the uCF and aCF could get the same frame rate by the parallel computing platforms (e.g., GPU and FPGA).

VI. CONCLUSION

We present a united coherence factor (uCF) using both spatial and angular information for CPWC and evaluate the performance by the metrics FWHM, CR and gCNR in different imaging datasets. For simulated images, the CR improvements are over 80%. In the phantom images, the maximum improvements of FWHM and CR are 10% and 105%, respectively. In the *in vivo* study, the CR and gCNR of the artery are increased by 133% and 35% and uCF delivers the sharpest vessel boundary. To compare the core differences, the sCF and aCF methods are also presented in this paper. uCF is superior in the lateral resolution and contrast among the beamformers. In addition to the tissue imaging, the uCF also performs best in the power Doppler experiment. It could improve the power Doppler imaging quality compared to the conventional methods, which is further verified by the Doppler image and spatial similarity matrix. Thus, the proposed method (uCF) has the potential to be applied in CPWC.

REFERENCES

[1] G. Montaldo, M. Tanter, J. Bercoff, N. Benech, and M. Fink, "Coherent plane-wave compounding for very high frame rate ultrasonography and transient elastography," *IEEE Trans. Ultrason., Ferroelectr., Freq. Control*, vol. 56, no. 3, pp. 489–506, Mar. 2009.

[2] J. Bercoff, G. Montaldo, T. Loupas, D. Savery, F. Mézière, M. Fink, and M. Tanter, "Ultrafast compound Doppler imaging: Providing full blood flow characterization," *IEEE Trans. Ultrason., Ferroelectr., Freq. Control*, vol. 58, no. 1, pp. 134–147, Jan. 2011.

[3] J. Lu and J. Greenleaf, "Pulse-echo imaging using a nondiffracting beam transducer," *Ultrasound Med. Biol.*, vol. 17, pp. 81–265, Jan. 1991.

[4] L. Sandrin, S. Catheline, M. Tanter, X. Hennequin, and M. Fink, "Time-resolved pulsed elastography with ultrafast ultrasonic imaging," *Ultrason. Imag.*, vol. 21, pp. 72–259, Jan. 1999.

[5] J. Bercoff, "Ultrafast ultrasound imaging," in *Ultrasound Imaging-Medical Applications*. Aug. 2011, pp. 3–24.

[6] C. Demene, T. Deffieux, M. Pernot, B.-F. Osmanski, V. Biran, J.-L. Gennisson, L.-A. Sieu, A. Bergel, S. Franqui, J.-M. Correas, I. Cohen, O. Baud, and M. Tanter, "Spatiotemporal clutter filtering of ultrafast ultrasound data highly increases Doppler and fUltrasound sensitivity," *IEEE Trans. Med. Imag.*, vol. 34, no. 11, pp. 2271–2285, Nov. 2015.

[7] J. Baranger, B. Arnal, F. Perren, O. Baud, M. Tanter, and C. Demene, "Adaptive spatiotemporal SVD clutter filtering for ultrafast Doppler imaging using similarity of spatial singular vectors," *IEEE Trans. Med. Imag.*, vol. 37, no. 7, pp. 1574–1586, Jul. 2018.

[8] C. Chen, G. A. G. M. Hendriks, R. J. G. van Sloun, H. H. G. Hansen, and C. L. de Korte, "Improved plane-wave ultrasound beamforming by incorporating angular weighting and coherent compounding in Fourier domain," *IEEE Trans. Ultrason., Ferroelectr., Freq. Control*, vol. 65, no. 5, pp. 749–765, May 2018.

[9] S. M. Hverven, O. M. H. Rindal, A. Rodriguez-Molares, and A. Austeng, "The influence of speckle statistics on contrast metrics in ultrasound imaging," in *Proc. IEEE Int. Ultrason. Symp. (IUS)*, Sep. 2017, pp. 1–4.

[10] J. Capon, "High-resolution frequency-wavenumber spectrum analysis," *Proc. IEEE*, vol. 57, no. 8, pp. 1408–1418, Aug. 1969.

[11] J. F. Synnevag, A. Austeng, and S. Holm, "Adaptive beamforming applied to medical ultrasound imaging," *IEEE Trans. Ultrason., Ferroelectr., Freq. Control*, vol. 54, no. 8, pp. 1606–1613, Aug. 2007.

[12] N. Q. Nguyen and R. W. Prager, "A spatial coherence approach to minimum variance beamforming for plane-wave compounding," *IEEE Trans. Ultrason., Ferroelectr., Freq. Control*, vol. 65, no. 4, pp. 522–534, Apr. 2018.

[13] B. M. Asl and A. Mahloojifar, "Eigenspace-based minimum variance beamforming applied to medical ultrasound imaging," *IEEE Trans. Ultrason., Ferroelectr., Freq. Control*, vol. 57, no. 11, pp. 2381–2390, Nov. 2010.

[14] P.-C. Li and M.-L. Li, "Adaptive imaging using the generalized coherence factor," *IEEE Trans. Ultrason., Ferroelectr., Freq. Control*, vol. 50, no. 2, pp. 128–141, Feb. 2003.

[15] J. Camacho, M. Parrilla, and C. Fritsch, "Phase coherence imaging," *IEEE Trans. Ultrason., Ferroelectr., Freq. Control*, vol. 56, no. 5, pp. 958–974, May 2009.

[16] R. Mallart and M. Fink, "The van Cittert-Zernike theorem in pulse echo measurements," *J. Acoust. Soc. Amer.*, vol. 90, no. 5, pp. 2718–2727, Nov. 1991.

[17] D.-L. Liu and R. C. Waag, "About the application of the van cittert-zernike theorem in ultrasonic imaging," *IEEE Trans. Ultrason., Ferroelectr., Freq. Control*, vol. 42, no. 4, pp. 590–601, Jul. 1995.

[18] M. A. Lediju, G. E. Trahey, B. C. Byram, and J. J. Dahl, "Short-lag spatial coherence of backscattered echoes: Imaging characteristics," *IEEE Trans. Ultrason., Ferroelectr., Freq. Control*, vol. 58, no. 7, pp. 1377–1388, Jul. 2011.

[19] C. K. Liao, M. L. Li, and P. C. Li, "Optoacoustic imaging with synthetic aperture focusing and coherence weighting," *Opt. Lett.*, vol. 29, no. 21, pp. 2506–2508, Nov. 2004.

[20] Y. L. Li and J. J. Dahl, "Coherent flow power Doppler (CFPD): Flow detection using spatial coherence beamforming," *IEEE Trans. Ultrason., Ferroelectr., Freq. Control*, vol. 62, no. 6, pp. 1022–1035, Jun. 2015.

[21] Y. L. Li and J. J. Dahl, "Angular coherence in ultrasound imaging: Theory and applications," *J. Acoust. Soc. Amer.*, vol. 141, no. 3, pp. 1582–1594, Mar. 2017.

[22] Y. Wang, C. Zheng, H. Peng, and C. Zhang, "Coherent plane-wave compounding based on normalized autocorrelation factor," *IEEE Access*, vol. 6, pp. 36927–36938, 2018.

[23] A. L. Hall, K. E. Thomenius, I. L. J. Thomas, and K. W. Rigby, "Method and apparatus for coherence imaging," U.S. Patents, 6 071 240 A, Jun. 6, 2000.

[24] J. Zhao, Y. Wang, X. Zeng, J. Yu, B. Y. S. Yiu, and A. C. H. Yu, "Plane wave compounding based on a joint transmitting-receiving adaptive beamformer," *IEEE Trans. Ultrason., Ferroelectr., Freq. Control*, vol. 62, no. 8, pp. 1440–1452, Aug. 2015.

[25] J. A. Jensen, "Field: A program for simulating ultrasound systems," in *Proc. 10th Nordicbaltic Conf. Biomed. Imag.*, vol. 4, 1996, pp. 351–353.

[26] J. A. Jensen and N. B. Svendsen, "Calculation of pressure fields from arbitrarily shaped, apodized, and excited ultrasound transducers," *IEEE Trans. Ultrason., Ferroelectr., Freq. Control*, vol. 39, no. 2, pp. 262–267, Mar. 1992.

[27] K. F. Üstüner and G. L. Holley, "Ultrasound imaging system performance assessment," in *Proc. AAPM Annu. Meeting*, 2003, pp. 1–33.

[28] A. Rodriguez-Molares, O. M. H. Rindal, J. D'hooge, S.-E. Masoy, A. Austeng, M. A. L. Bell, and H. Torp, "The generalized Contrast-to-Noise ratio: A formal definition for lesion detectability," *IEEE Trans. Ultrason., Ferroelectr., Freq. Control*, vol. 67, no. 4, pp. 745–759, Apr. 2020.

[29] B. Denarie, T. A. Tangen, I. K. Ekroll, N. Rolim, H. Torp, T. Bjastad, and L. Lovstakken, "Coherent plane wave compounding for very high frame rate ultrasonography of rapidly moving targets," *IEEE Trans. Med. Imag.*, vol. 32, no. 7, pp. 1265–1276, Jul. 2013.

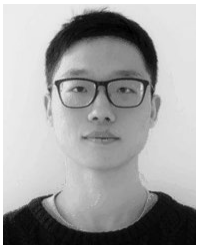

CHEN YANG received the B.E. degree in biomedical engineering from Xi'an Jiaotong University, Xi'an, China, in 2016. He is currently pursuing the Ph.D. degree with the University of Science and Technology of China.

His research interests include adaptive beamforming and medical ultrasound imaging.

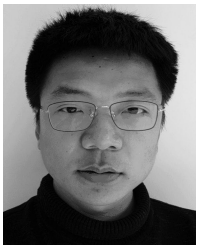

JIE XU received the M.S. degree in mechanical and electronic engineering from the University of Chinese Academy of Sciences, China, in 2014. He is currently doing research on medical ultrasound systems with the Suzhou Institute of Biomedical Engineering and Technology, Suzhou, China. His research interests include ultrasonic hardware and system design.

YIWEN XU received the B.E. degree in biomedical engineering from Xi'an Jiaotong University, Xi'an, China, in 2015, and the M.E. degree in optical engineering from the University of Chinese Academy of Science, in 2018. Her research interests include clutter suppression and ultrasound Doppler imaging.

YAOYAO CUI (Member, IEEE) received the M.S. and Ph.D. degrees in biomedical engineering from Xi'an Jiaotong University, Xi'an, China, in 1999 and 2002, respectively.

In 2003, she joined the CREATIS, INSA de Lyon, Villeurbanne, France, as a Postdoctoral Researcher and was appointed by the Medical Vision Laboratory as a Postdoctoral Research Associate with the University of Oxford, Oxford, U.K., in 2004. In 2007, she was a Research Fellow with the University of Dundee, Dundee, U.K. Since 2011, she has been a Hundred Talents Professor with the Suzhou Institute of Biomedical Engineering and Technology, Suzhou, China, where she is currently the Director of the Medical Ultrasound Department. Her research interests include ultrasound imaging and ultrasound bioeffects.

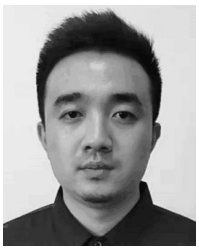

YANG JIAO received the B.S. and M.S. degrees from the Nanjing University of Aeronautics and Astronautics, Nanjing, China, in 2010 and 2013, respectively. He is currently doing research on medical ultrasound imaging with the Suzhou Institute of Biomedical Engineering and Technology, Suzhou, China. His research interests include ultrasonic imaging and system design.